 doi:10.20944/preprints202002.0174.v1

Article

Evaluating IEEE 802.15.4g SUN for Dependable Low-Power Wireless Communications In Industrial Scenarios

Pere Tuset-Peiró [1,*], Ruan D. Gomes[2], Pascal Thubert[3], Xavier Vilajosana[1]

[1] Wireless Networks (WiNe) Research Laboratory, Internet Interdisciplinary Institute (IN3), Universitat Oberta de Catalunya (UOC), Castelldefels, Spain.
[2] Research Group on Communications Systems and Information Processing, Instituto Federal de Educação, Ciência e Tecnologia da Paraíba (IFPB), Campus Campina Grande, Brazil.
[3] Cisco Systems France S.à.r.l., Issy-les-Moulineaux, France.
* Correspondence: Pere Tuset-Peiró. Estudis d'Informàtica, Multimèdia i Telecomunicació. Universitat Oberta de Catalunya. Rambla del Poblenou 156, 08018 Barcelona, Spain. Email: peretuset@uoc.edu.

Abstract: In this article we present a deployment of 11 nodes using the three different SUN (Smart Utility Network) modulation schemes, as defined in the IEEE 802.15.4-2015 standard. The nodes were deployed in a 110.044 m^2 warehouse for 99 days, and the resulting dataset contains a total of 10.710.868 measurements with RSSI (Received Signal Strength Indicator), CCA (Clear Channel Assessment) and PDR (Packet Delivery Ratio) values. The analyzed results show a high variability in average RSSI (i.e., between -82.1 dBm and -101.7 dBm) and CCA (i.e., between -111.2 dBm and -119.9 dBm) values, which are caused by the effects of multi-path propagation and external interference. Despite being above the sensitivity limit for each modulation, this values result in poor average PDR values (i.e., from 65.9% to 87.4%), indicating that additional schemes are required for low-power wireless communications to meet the dependability requirements of industrial applications. For that purpose, we also introduce the concept of modulation diversity, which can be combined with packet repetition to meet such requirements (i.e., PDR>99%) while minimizing the energy expenditure of nodes and meeting regulatory constraints.

Keywords: IEEE 802.15.4g; Smart Utility Networks; Low-Power; Wireless; Communications; Dependable; Predictable; Reliable; Available; Industrial; Dataset.

1. Introduction

Industrial and smart grid applications require dependable transmissions for monitoring and control operations, which means reliable, available and timely delivery of packets [1]. In wired networks this kind of dependability is achieved using a central path computation entity with a God's view. However, this model cannot be simply adapted to wireless networks, for two main reasons [2]. First, wireless communications are subject to propagation (i.e., the Fresnel zone is typically blocked) and interference (i.e., these networks operate in unlicensed bands) effects. Second, radio conditions may change faster (i.e., mobile nodes or dynamic environment cause multi-path fading) than a centralized engine can adapt and reprogram, in particular when the controller is distant or when connectivity is limited.

To guarantee dependability in such adverse conditions, the RAW (Reliable and Available Wireless) WG (Working Group) is currently being formed at the IETF (Internet Engineering Task Force) [3]. RAW enables parallel transmissions over heterogeneous media and multiple hops, and leverages the PAREO functions [4], which stand for Packet Replication, ARQ (Automatic Repeat Request), Replication, Elimination and re-Ordering. In addition, RAW separates the routing time scale, at which a complex path is recomputed, from the forwarding time scale, at which the forwarding decision is taken for an individual packet. Hence, the RAW problem is to decide, within the redundant solutions that

 doi:10.20944/preprints202002.0174.v1

are proposed by the routing, which will be used for each individual packet to provide a dependable service while minimizing the waste of resources. That is, a RAW solution would consist of a set of protocols that evaluate the media in real-time, and that control the use of redundancy and diversity attributes that are available along the path.

Given the rising interest of dependable low-power wireless communications for industrial and smart grid applications, there are various studies that have recently focused on analysing the performance of IEEE 802.15.4g SUN (Smart Utility Network) modulations, namely SUN-FSK (Frequency Shift Keying), SUN-OQPSK (Offset Quadrature Phase-Shift Keying) and SUN-OFDM (Orthogonal Frequency Division Multiplexing), as defined in the latest revision of the IEEE 802.15.4 standard [5]. For example, in [6], [7] and [8] the authors study the suitability of IEEE 802.15.4g SUN modulations for smart metering utility networks. More recently, in [9] and [10] the authors study the suitability of IEEE 802.15.4g in smart building and environmental monitoring scenarios, respectively. However, none of these studies have conducted a deployment in an industrial scenario to evaluate the real-world performance of these technologies for a long period of time, and demonstrate its benefits and drawbacks.

In this paper we fill this gap by presenting the deployment of 11 nodes using the IEEE 802.15.4g SUN modulations for 99 days in a 110.044 ^{2} warehouse, and the analysis of the resulting dataset, which contains 10.710.868 measurements of RSSI (Received Signal Strength Indicator), CCA (Clear Channel Assessment) and PDR (Packet Delivery Ratio) values. The results show large variability in average RSSI (i.e., between -82.1 dBm and -101.7 dBm) and CCA (i.e., between -111.2 dBm and -119.9 dBm) values caused by multi-path propagation and external interference effects, leading to poor PDR values (i.e., from 65.9% to 87.4%) despite the fact that nodes are well above the sensibility limit for each modulation. To the best of our knowledge, this is the first paper to present a large dataset using IEEE 802.15.4g SUN modulations in an industrial environment, and we expect that the data gathered will enable researchers and practitioners to study alternatives to enhance dependability properties of low-power wireless communications in the context of the RAW WG at the IETF.

The remaining of this article is organized as follows. Section 2 provides an overview of the SUN modulations that are standardized in IEEE 802.15-2015. Section 3 describes the environment, the hardware and the network operation used for the deployment. Section 4 presents the dataset and analyzes the results obtained from the measurements campaign. Section 5 discusses the results and proposes *modulation diversity* as a means to combat the effects of multi-path propagation and external interference, and to achieve the dependability required for industrial and smart grid applications. Finally, Section 6 concludes the article.

2. Overview of IEEE 802.15.4g

The IEEE 802.15.4 standard [5] was first released in May 2003 and defined a PHY (PHYsical) layer and a MAC (Medium Access Control) layer for LR-WPAN (Low Rate Wireless Personal Area Networks). At the PHY layer, the standard employed the DSSS-OQPSK (Direct Sequence Spread Spectrum - Offset Quadrature Phase Shift Keying) modulation and provides data rates of 20 kbps and 40 kbps in the Sub-GHz bands (868 MHz in Europe, 915 MHz in America), respectively, and of 250 kbps in the 2.4 GHz band (available world-wide. The selected modulation provided a good trade-off between radio transceiver complexity, robustness, energy consumption, and communication range [10]. At the MAC layer, the standard defined slotted/synchronized and unslotted/unsynchronized operation based on the CSMA/CA (Carrier Sense Multiple Access with Collision Avoidance) channel access mechanism to trade off bandwidth, latency and energy consumption of the devices.

The adoption of the IEEE 802.15.4 standard by different low-power wireless technologies has promoted the revision of the standard three times (i.e., in 2006, 2011 and 2015) in order to clarify the operation and to add new features to both the PHY and MAC layers. For example, the 2015 standard revision adopted the MAC layer proposals defined in the IEEE 802.15.4e-2012 [11] amendment. Among others, this amendment defined the TSCH (Time Slotted Channel Hopping), a channel access

 doi:10.20944/preprints202002.0174.v1

mechanism that combines TDMA (Time Division Multiple Access) and FDMA (Frequency Division Multiple Access) to support industrial requirements, including reliable packet delivery (i.e. 99.999%) in adverse conditions, such as multi-path propagation and external interference. Similarly, the IEEE 802.15.4-2015 standard revision included three new physical layers targeted to SUN (Smart Utility Network) applications, as defined in the IEEE 802.15.4g-2012 [12] amendment. The SUN-FSK and SUN-OQPSK modulations focus on maintaining backwards compatibility with previous standards and commercially available transceivers, whereas the SUN-OFDM is focused on adding robustness and improving spectrum efficiency at the physical layer.

In the following subsections we present the operation of SUN-FSK, SUN-OQPSK and SUN-OFDM, as these are the physical layers that were used in the deployment described in this article.

2.1. SUN-FSK

The SUN-FSK modulation has two main advantages: the first one is the good power efficiency, due to the constant envelope of the signal, and the low implementation complexity, and the second one is the compatibility with legacy systems. For example, most of the deployed systems for smart metering in the United States are based on FSK modulation schemes, mainly the ones that use the 902-928 MHz frequency band.

The SUN-FSK may be used in several frequency bands, which makes it suitable for different regions. In particular, the 2.4 GHz band is allowed worldwide, and the 863–870 MHz band is allowed in Europe. Three different operation modes are defined for each frequency band. The operation mode defines modulation and channel parameters, such as the modulation type (2-FSK or 4-FSK), the channel spacing, and the modulation index.

In the 863–870 MHz band, three data rates are supported depending on the operation mode selected: 50 kbps, 100 kbps, and 200 kbps. The higher data rate is achieved when using 4-FSK. However, only the Mode 1, which uses 2-FSK, with a data rate of 50 kbps, is mandatory. In the deployment described in this article, the Mode 1 was used. In this mode, the total number of channels is 34, with a channel spacing of 200 kHz.

At the physical layer, the PSDU (PHY Service Data Unit) can be optionally processed by a Forward Error Correction (FEC) encoder. Two types of FEC may be applied: a recursive and systematic code (RSC) or a nonrecursive and nonsystematic code (NRNSC). FEC shall be employed on the PHY header (PHR) and PSDU bits, applying a 1/2-rate coding with constraint length $K = 4$. Interleaving shall be employed in conjunction with NRNSC coding, and may also be employed with RSC coding. The use of data whitening is optional.

The SUN-FSK Physical Protocol Data Unit (PPDU) is composed by a synchronization header (SHR) – with a preamble and a SFD (Start of Frame Delimiter), a PHR of 16 bits, and a payload of up to 2047 bytes. In the PHR, the Frame Check Sequence (FCS) length is defined, as well as the frame length. There is one bit to indicate if data whitening is used, and other one to indicate the occurrence of a mode switching. Mode switch is a mechanism that allows changing the symbol rate or modulation scheme used by the radios.

2.2. SUN-OQPSK

The OQPSK modulation was introduced in the first version of the IEEE 802.15.4 standard, in 2003, only for the 2.4 GHz band, and providing a bit rate of 250 kbps. In the IEEE 802.15.4g, other modes of use were defined, allowing the use of OQPSK modulation also in other frequency bands, and for bitrates varying from 6.25 to 500 kbps. The SUN-OQPSK employs Direct Sequence Spread Spectrum (DSSS), and with different spreading factors. The use of DSSS allows a better resistance to interference. For some bands, it is possible to use an alternative spreading mode, called Multiplexed DSSS (MDSSS).

The PPDU of the SUN-OQPSK frame is composed by a SHR, a PHR, and the PHY payload (PSDU). The symbol rate is defined as the bit rate of the SHR. Other important parameters are defined in the PHR, such as the spreading mode, and the rate mode. Up to four rate modes are supported for each

 doi:10.20944/preprints202002.0174.v1

frequency band, but only the rate mode 0 is mandatory. The bit-to-chip mapping used for the SHR and PHR fields depends on the frequency band, and the mapping used for the payload depends on the rate mode. In Mode 3 of the sub-GHz bands, DSSS is not used for the payload, and it is possible to achieve a higher data rate. For the 2.4 GHz band DSSS is used for the payload in all rate modes.

The use of FEC is mandatory for the PHR field. When using DSSS as the spreading mode, FEC shall also be applied to the PSDU bits, with a 1/2-rate convolutional coding, with constraint length $K = 7$. For spreading mode set to MDSSS, FEC is optional, depending on the rate mode. Interleaving shall be employed in conjunction with FEC, to improve robustness against burst errors and to break correlation of consecutive bits.

2.3. SUN-OFDM

The SUN-OFDM was first defined in the IEEE 802.15.4g standard, and after incorporated in the IEEE 802.15.4-2015. It was defined to provide high data rates and long range, while dealing with interference and multi-path fading problems. Unlike FSK and OQPSK, OFDM have not been widely used for low-power wireless communications, due to the stringent processing, memory and energy consumption requirements.

The SUN-OFDM may be used in different frequency bands (both Sub-GHz and 2.4 GHz), and provides data rates from 50 kbps to 800 kbps. The sub-carrier spacing is constant and is equal to 10416-2/3 Hz, while the symbol rate is equal to 8-1/3 ksymbol/s (a symbol period of 120 μs). Four different options are defined, each one with a different number of active tones. For each option, a set of Modulation and Coding Schemes (MCS), numbered from 0 to 6, may be used. If a device supports a given option, it has to support all BPSK and QPSK modulations and all MCS for that option. The support to QAM (Quadrature Amplitude Modulation) is optional.

The MCS determines the scheme used to modulate the sub-carriers (BPSK, QPSK or 16-QAM), whether frequency repetition is applied (i.e., 4x, 2x or no frequency repetition) and the FEC coding rate (1/2 or 3/4). Thus, the effective data rate depends on the used MSC. For example, for Option 2, which uses 52 active tones and was the option evaluated in this paper, the effective data rate may vary from 50 kbps, when using BPSK, a coding rate of 1/2, and 4x frequency repetition, to 800 kbps, when using QAM, with a coding rate of 1/2, and no frequency repetition.

The PPDU of the SUN-OFDM is composed by a SHR, a PHR, and the payload. The SHR has a preamble, and the PHR contains the information about the configuration used to transmit the payload. Both SHR and PHR are transmitted using the lowest supported MSC for the option being used. The maximum length of the payload is 2047 bytes, which allows transmitting a complete IPv6 packet without fragmentation.

3. Deployment overview

This section presents the environment, introduces the hardware, and describes the network operation of the deployment.

3.1. Overview

The network has been deployed in a warehouse located in Madrid (Spain), as depicted in Figure 1. The warehouse is built with steel and concrete, and measures 451 m x 244 m (area 110.044 m^2). As shown in Figure 2, a total of 11 nodes (green) and 1 gateway (orange) have been placed in the warehouse. The gateway has been located near the warehouse entrance (bottom, center), whereas the nodes have been placed at different distances and heights with the aim to measure temperature and relative humidity distribution. Table 3 shows the node identifiers (last two bytes of EUI-64 address) and the distance to the gateway, which is comprised between 34.0 meters and 273.5 meters.

Preprints (www.preprints.org) | NOT PEER-REVIEWED | Posted: 13 February 2020 doi:10.20944/preprints202002.0174.v1

(a) (b) (c)

Figure 1. Warehouse environment overview. Notice how the warehouse is cluttered with large metal objects and tall metal structures, creating an environment subject to multi-path propagation conditions.

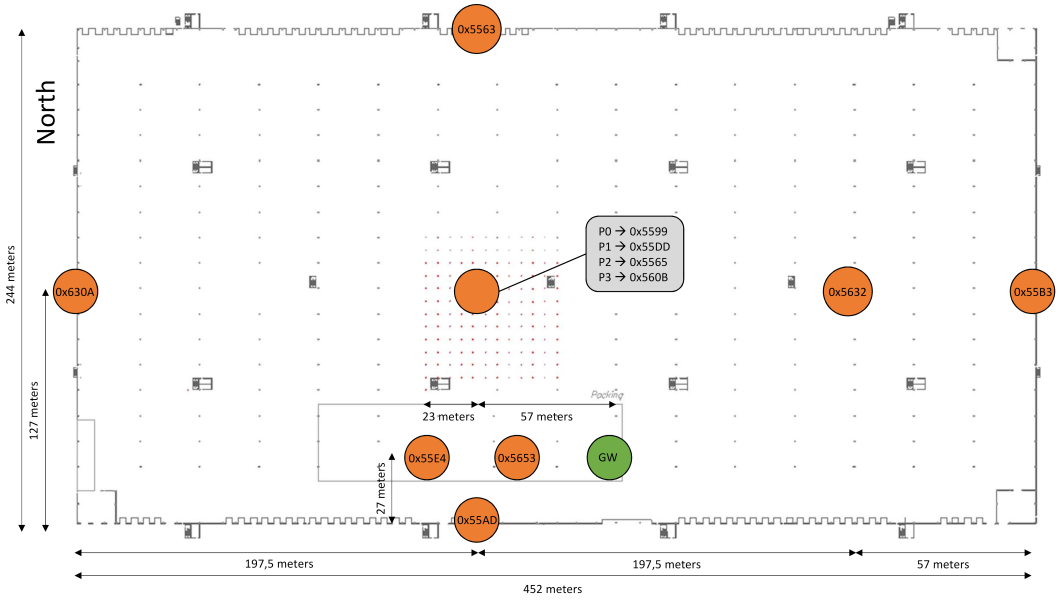

Figure 2. Map of nodes (orange) and gateway (green) deployed inside the warehouse. Notice that 4 nodes are deployed at the same position in the middle of the warehouse, but at four different floor levels (i.e., P0, P1, P2 and P3).

3.2. Hardware

Both the nodes and the gateway are implemented using the OpenMote-B board [13,14], as shown in Figure 3a. The OpenMote-B board is equipped with a Texas Instruments CC2538 SoC (System on Chip) and a Microchip AT86RF215 radio transceiver. The CC2538 [15] includes an ARM Cortex-M3 micro-controller (32 MHz, 32 kB RAM, 512 kB Flash) and a radio transceiver compatible with the IEEE 802.15.4-2006 standard. The AT86RF215 [16] is a dual-band (Sub-GHz and 2.4 GHz) radio transceiver compatible with the IEEE 802.15.4-2015 standard, which supports all Multi-Rate PHY options defined in the IEEE 802.15.4g-2012 amendment (i.e., SUN-FSK, SUN-OQPSK and SUN-OFDM).

For the nodes the OpenMote-B is coupled with the OpenMote-Sensors board, shown in Figure 3b. The OpenMote-Sensors is a carrier board equipped with the Bosch BME280 [17] and the Texas Instruments OPT3001 [18] sensors. The Bosch BME280 sensor can measure temperature, relative

Preprints (www.preprints.org) | NOT PEER-REVIEWED | Posted: 13 February 2020 doi:10.20944/preprints202002.0174.v1

EUI-64 (last 2-bytes)	Distance (m)	Height (m)	Cluster group
56-53	34.0	12.0	Close
55-AD	63.0	2.0	Close
55-E4	80.0	6.0	Close
55-99	115.1	2.0	Medium
55-DD	115.1	6.0	Medium
55-65	115.1	10.0	Medium
56-0B	115.1	14.0	Medium
56-32	172.5	2.0	Far
55-B3	221.4	2.0	Far
55-63	224.4	2.0	Far
63-0A	273.5	2.0	Far

Table 1. Node identifier (EUI-64), distance to gateway and height. Notice that for evaluation purposes nodes are grouped into clusters (i.e., *close*, *medium* and *far*) according to their distance to the gateway.

humidity and pressure, whereas the OPT3001 can measure ambient light. The nodes are enclosed in a custom 3D-printed case that exposes the sensors and the SMA antenna connectors, but hides the USB connector for protection. Each node is powered by a pair of 2xAA batteries in series, providing 2.4 V and containing a nominal charge of 2000 mAh. The laboratory measurements previous to the deployment show an average consumption of 0.2 mA during operation (described in Section 3.3), allowing the boards to remain operative for about 1 year.

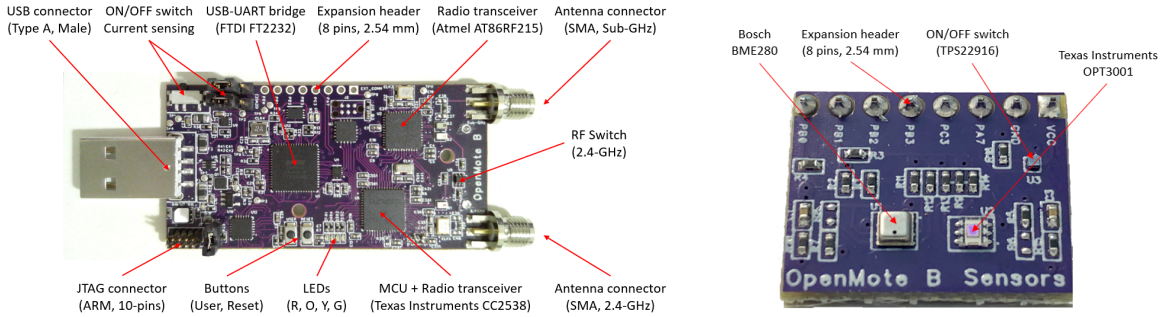

(a) OpenMote-B board. **(b)** OpenMote-Sensors board.

Figure 3. OpenMote-B (left) and OpenMote-Sensors (right) boards.

The gateway, depicted in Figure 4, is composed of a Raspberry Pi 3B+ SBC (Single Board Computer) connected to three OpenMote-B boards that act as receivers, and Huawei E3531 HSPA+ modem to provide Internet access. Power to the gateway is supplied through an internal PSU (Power Supply Unit), which translates the 220 VAC to 5 VDC. The gateway runs GNU/Linux and executes a Python script that reads the packets from each OpenMote-B receiver, converts the raw packet to a JSON payload, and forwards it to the cloud back-end using MQTT (Message Queue Telemetry Transport).

3.3. Network operation

Figure 5 depicts the network setup, with the nodes on the left and the gateway with Internet access on the right.

Nodes operate on a 60 seconds period with an active time of 1750 ms, as depicted in Figure 6. During the active period the nodes sample the environmental sensors (100 ms) and then perform 3 transmit cycles. At each transmit cycle the node transmits 3 different packets, one with each of the SUN modulations (i.e., SUN-FSK, SUN-OQPSK and SUN-OFDM). Between two consecutive packets in a transmit cycle there is a 50 ms inter-packet delay. Also, between the 1st and 2nd cycle there is a 100 ms delay, whereas between the 2nd and 3rd cycle there is a 200 ms delay.

Preprints (www.preprints.org) | NOT PEER-REVIEWED | Posted: 13 February 2020 doi:10.20944/preprints202002.0174.v1

Figure 4. Gateway setup with 3xOpenMote-B boards, 1xRaspberry Pi 3B+ (not displayed) and a Huawei E3531 HSPA+ modem.

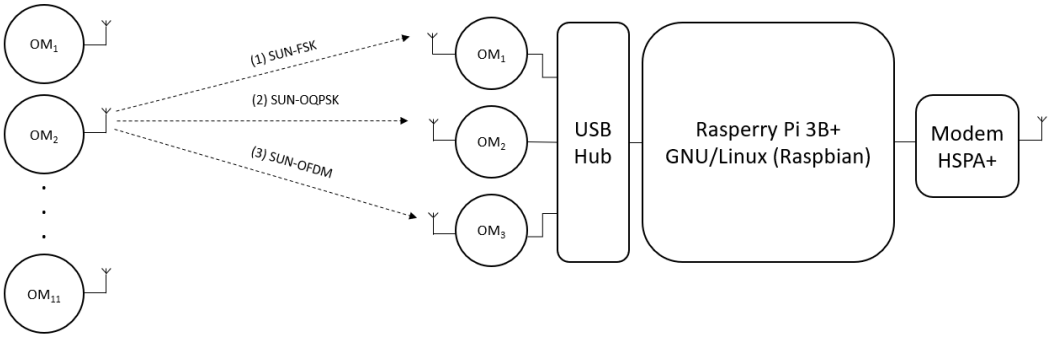

Figure 5. Hardware setup.

Before each packet transmission nodes execute a CSMA/CA (Carrier Sense Multiple Access / Collision Avoidance) protocol with CCA (Clear Channel Assessment) to determine if the channel is busy. That is, prior to transmitting the radio samples the channel to determine the energy present. If the energy is below the threshold for the current modulation the CSMA/CA succeeds and the packet is loaded to the radio transceiver and transmitted subsequently. Otherwise, if the energy is above the threshold for the current modulation, the transmission is delayed for a random back-off time between 0 and 10 ms. The mode draws a random number between 0 and 100 representing the number of slots and each slot being 100 *us*. The CCA threshold values for SUN-FSK, SUN-OQPSK and SUN-OFDM have been determined experimentally and have been set to -94 dBm, -93 dBm and -91 dBm, respectively.

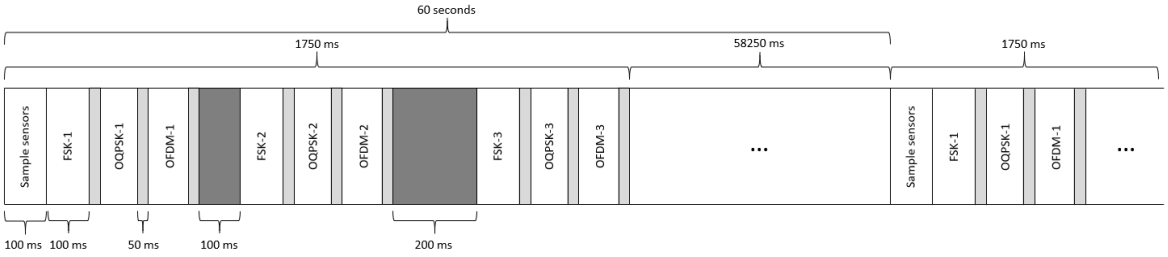

Figure 6. Sensing and packet transmission timeline. Sensors are sampled once and each packet is repeated 9 times (3 times for each modulation).

The configuration parameters for the different IEEE 802.15-4 SUN modulations used to transmit packets are summarized in Table 2. As it can be observed, all modulations provide an effective data rate of 50 kbps, but they trade-off link budget and occupied bandwidth. As it can be observed, SUN-FSK provides a good link budget (i.e., 129 dB) and the largest number of channels (i.e.,34) thanks to its narrow bandwidth occupation (i.e., 200 kHz). In contrast, SUN-OQPSK provides the highest link

Preprints (www.preprints.org) | NOT PEER-REVIEWED | Posted: 13 February 2020 doi:10.20944/preprints202002.0174.v1

budget (i.e, 131 dB) at the expense of bandwidth occupation (i.e., 1300 kHz). Finally, SUN-OFDM provides a trade-off between channel occupation (i.e., 800 kHz) and link budget (i.e., 120 dB). Notice that for all the SUN modulations the transmit power of the AT86RF215 radio transceiver is set to its maximum value. However, there is a 6 dB offset between the value of the transmit power and the actual transmit power of the radio transceiver depending on the selected modulation. Hence, for SUN-FSK and SUN-OQPSK the packets are transmitted with 15 dBm, whereas for SUN-OFDM they are transmitted with 9 dBm.

	SUN-FSK	**SUN-OQPSK**	**SUN-OFDM**
Name	Mode 1	Mode 3	Option 2 MCS0
Data rate (kbps)	50	50	50
Modulation type	BFSK	OQPSK	BPSK
Modulation index	1.0	N/A	N/A
Chip rate (kchips/s)	N/A	100	N/A
Spreading mode	N/A	SHR:(32,1)-DSSS PHR:(8,1)-DSSS PSDU: none	N/A
Pilots Total/Data/Pilot	N/A	N/A	52/48/4
Center frequency (MHz)	863.125	868.3	863.425
Channel spacing (kHz)	200	1300	800
Available channels	34	3	8
Transmit power (dBm)	15	15	9
Sensitivity (dBm)	-114	-116	-111
CCA Threshold (dBm)	-94	-93	-91
Notes	FEC: yes	Coding rate: 1/2 Interleaver: yes	Coding rate: 1/2 Freq. repetition: 4x

Table 2. IEEE 802.15.4-2015 SUN modes used in the deployment.

In terms of payload, each packet contains the fields depicted in Figure 7, as summarized next:

- The `PAN_ID` field is 2 bytes and is set to `0xCAFE` for all packets being transmitted. The gateway filters all packets that are not received with such value.
- The `EUI_16` field is 2 bytes and contains the last two bytes of the EUI-64 address of the devices transmitting the packet.
- The `TX_MODE` field is 1 byte and refers to the modulation being used to transmit the packet: SUN-FSK (0), SUN-OQPSK (1) and SUN-OFDM (2).
- The `TX_COUNTER` field is 1 byte and indicates the packet repetition within the current period, i.e., 1, 2 or 3.
- The `PACKET_COUNTER` field is 4 bytes and is an absolute sequence number to allow for packet identification and eventual node resets.
- The `TEMPERATURE`, `HUMIDITY`, `PRESSURE` and `LIGHT` fields are 2 bytes each and are devoted to store the sensor measurements. Prior to transmitting the raw values are converted to their respective values and multiplied by 10 to provide single-digit decimal resolution.

Preprints (www.preprints.org) | NOT PEER-REVIEWED | Posted: 13 February 2020 doi:10.20944/preprints202002.0174.v1

- The `CSMA_RETRIES` value is 1 byte and indicates the number of times that the CSMA/CA process was repeated before a transmission is allowed.
- The `CSMA_RSSI` value is 1 byte and indicates the RSSI level (dBm) that was measured during the CSMA/CA process.

LENGTH	PAN ID	EUI-16	TX MODE	TX COUNTER	PACKET COUNTER	TEMPERATURE	HUMIDITY	PRESSURE	LIGHT	CSMA RETRIES	CSMA RSSI
1 Byte	2 Bytes	2 Bytes	1 Byte	1 Byte	4 Bytes	2 Bytes	2 Bytes	2 Bytes	2 Bytes	1 Byte	1 Byte
0-255	0xCAFE		{0,1,2}	{0,1,2}	$\{0 - 2^{32}\text{-}1\}$						

Figure 7. Packet structure.

Notice that regardless of the modulation, the packet length is always 21 bytes. However, before transmission packets are encrypted using AES-128 and, hence, the length of the PSDU transmitted by each end-device is 32 bytes. Thus, considering that packets are transmitted at 50 kbps, each packet requires 5.12 ms to be transmitted. Since each node transmits 9 packets every minute and that there are 11 nodes in the network, the total channel occupation is 506.88 ms per minute (about 0.85%). Hence, considering the low occupation and the use of CSMA/CA prior to transmission, we do not expect a high impact in performance caused by self-interference.

4. Performance evaluation

This section presents a description of the dataset and conducts a statistical analysis of the RSSI, the CCA and the PDR values, which are defined as:

- **RSSI (Received Signal Strength Indicator)**: Average power (dBm) of a packet that has been received by the gateway.
- **CCA (Clear Channel Assessment)**: Average power (dBm) that a transmitter has sampled before transmitting a packet.
- **PDR (Packet Delivery Ratio)**: Percentage of packets that have been successfully received by the gateway within a given period of time.

4.1. Overview

The dataset can be found in a public GitHub repository[1] (https://github.com/wine-uoc/wisun_traces) and contains the data captured from the 11 nodes between July 31 and November 10, 2019 (103 days). However, due to external reasons (i.e., loss cellular connectivity) we do not have enough data for 4 days (20-21/08/2019 and 28-29/10/2019, respectively). Hence, the data analyzed only encompasses 99 days of the total.

Hence, the dataset is composed of 11 files formatted in CSV (Coma Separated Value), one for each sensor that has been deployed. The files are named `data_x.csv`, where `x` are the last two bytes of the EUI-64 node address, and each file contains 13 columns. The first 4 columns are independent of the modulation and contain the following fields:

- `day`: The day that the packet was received in `yyyy/mm/dd` format.
- `hour`: The hour that the packet was received in `hh/mm/ss` format.
- `pkt_number`: The number of the packet received.
- `pkt_retry`: The number of the packet retry (i.e., 0, 1, 2).

The next 9 columns contain 3 different fields that are repeated for each SUN modulation (i.e., FSK, OQPSK and OFDM):

[1] In addition to the data itself, the repository also contains all the Python/Jupyter scripts that have been used to generate the tables and figures presented in this article.

Preprints (www.preprints.org) | NOT PEER-REVIEWED | Posted: 13 February 2020 doi:10.20944/preprints202002.0174.v1

- `rssi`: The RSSI value (dBm) for the current packet received.
- `cca`: The CCA value (dBm) sampled before the current packet was transmitted.
- `cca_retries`: The number of retries before the transmission passed the CCA check and the packet was transmitted.

4.2. Data analysis

First, Table 3 shows the basic statistics (i.e., total packets received, mean RSSI, mean CCA and PDR) aggregated by node. As it can be observed, a total of 10710868 packets have been received out of 14113440 packets (i.e., 11 nodes, 99 days, 24 hours, 60 minutes, 9 messages) transmitted by all the nodes during the deployment, representing an aggregate PDR (Packet Delivery Ratio) of 75.9%. However, nodes experience different communication impairments (i.e., multi-path propagation and external interference), leading to a per-node PDR that ranges between 65.9% and 87.4% depending on the distance and the noise levels.

In that regard, it is important to notice that even nodes that are close together experience high RSSI and PDR variability. For example, nodes `55-99`, `55-DD`, `55-65` and `56-0B` are at the same distance from the gateway (i.e., 115.1 m), but have RSSI values ranging between 85.3 dBm and 96.2 dBm, and average PDR ranging from 67.9% to 85.1%.

Given these results we have decided to cluster the nodes according to the distance (d) to the gateway, allowing to make comparisons within similar groups. In particular, we have defined three groups of nodes: (1) nodes that are *close* to the gateway (i.e., $d < 80$ m: `56-53`, `55-AD` and `55-E4`), (2) nodes that are at a *medium* distance from the gateway (i.e., $80 \leq d < 150$ m: `55-99`, `55-DD`, `55-65` and `56-0B`) and, (3) nodes that are *far* from the gateway (i.e., $d \geq 150$ m: `56-32`, `55-B3`, `55-63` and `63-0A`).

As an example, in Table 3 we can observe that nodes of the *far* group present an average CCA value (-119.0 dBm) that is lower than those of the *close* group (-113.0 dBm). This can be explained by the fact that the gateway is located near the warehouse entrance, where other wireless technologies are known to be deployed and operating in the same Sub-GHz band (i.e., 868 MHz), creating interference. Moreover, we observe that nodes of the *close* group with higher CCA average have lower PDR values at the physical layer. For example, node `55-E4` has a CCA of -111.2 dBm and a PDR of 68.0%, whereas node `55-AD` has a CCA of -115.5 dBm and a PDR of 79.9%. This can be explained by the fact that nodes with higher CCA average values will refrain from transmitting more often due to the CCA threshold value defined in Table 2.

EUI-64 (2-bytes)	Received packets	RSSI (dBm)	CCA (dBm)	PDR (%)
`56-53`	924574	-84.0	-112.4	72.1
`55-AD`	1024664	-83.7	-115.5	79.9
`55-E4`	872200	-82.1	-111.2	68.0
`55-99`	897718	-96.2	-117.5	70.0
`55-DD`	1091950	-92.5	-117.3	85.1
`55-65`	1058746	-85.3	-118.3	82.5
`56-0B`	871477	-91.3	-118.4	67.9
`56-32`	1121696	-96.1	-119.9	87.4
`55-B3`	1076572	-95.0	-119.3	83.9
`55-63`	926221	-101.7	-118.1	72.2
`63-0A`	845050	-101.6	-119.0	65.9
Mean	10710868	-91.8	-117.0	75.9

Table 3. Node identifier (EUI-64), received packets, RSSI, CCA and PDR.

Table 4 shows the per-node RSSI, CCA and PDR values separated by modulation type. As it can be observed, the SUN-FSK provides the highest physical layer PDR (81.3%) compared to SUN-OQPSK (80.7%) and SUN-OFDM (65.7%). However, SUN-OQPSK provides the minimum standard deviation (6.6) compared to SUN-FSK (7.8) and SUN-OFDM (14.7). This can be explained because SUN-OQPSK

Preprints (www.preprints.org) | NOT PEER-REVIEWED | Posted: 13 February 2020 doi:10.20944/preprints202002.0174.v1

has a higher sensitivity (-116 dBm) compared to SUN-FSK (-114 dBm) and SUN-OFDM (-109 dBm), allowing to receive packets that are received with lower RSSI with higher probability.

In that regard, it is important to notice that the PDR at the physical layer is low despite the fact that the RSSI is well above the sensitivity limit for each modulation. For SUN-FSK the average RSSI of -87.1 dBm is only able to provide a PDR of 81.3% despite that the sensitivity limit is -114 dBm. Similarly, for SUN-OQPSK the average RSSI of -94.8 dBm can only provide a physical layer PDR of 80.7% with a sensitivity limit of -116 dBm. Finally, for SUN-OFDM the average RSSI of -93.4 dBm can only provide a physical layer PDR of 65.7% with a sensitivity limit of -111 dBm.

EUI-64 (2-bytes)	SUN-FSK			SUN-OQPSK			SUN-OFDM		
	RSSI (dBm)	CCA (dBm)	PDR (%)	RSSI (dBm)	CCA (dBm)	PDR (%)	RSSI (dBm)	CCA (dBm)	PDR (%)
56-53	-78.5	-118.5	71.7	-85.0	-114.6	75.7	-88.4	-104.0	68.8
55-AD	-76.8	-120.0	79.8	-89.6	-117.4	78.5	-84.7	-109.2	81.2
55-E4	-75.3	-117.6	66.8	-84.9	-113.2	70.3	-86.1	-102.8	66.8
55-99	-91.9	-121.6	77.6	-99.0	-119.7	77.0	-97.7	-111.3	55.2
55-DD	-86.9	-122.2	88.9	-96.1	-119.5	88.1	-94.5	-111.1	78.4
55-65	-79.8	-122.6	81.5	-85.9	-119.8	88.1	-90.1	-112.4	78.0
56-0B	-86.2	-122.5	74.4	-94.4	-120.4	74.7	-93.4	-112.4	54.6
56-32	-92.0	-123.2	93.9	-101.0	-122.4	89.4	-95.5	-114.0	79.0
55-B3	-93.4	-122.8	88.3	-96.8	-122.0	89.0	-94.9	-113.1	74.4
55-63	-99.6	-122.9	86.7	-106.2	-119.3	74.7	-99.4	-112.0	55.1
63-0A	-97.9	-122.7	84.8	-104.1	-121.5	82.2	-102.8	-112.7	30.6
Mean	-87.1	-121.5	81.3	-94.8	-119.1	80.7	-93.4	-110.5	65.7
Std. Dev.	8.2	1.8	7.8	7.2	2.8	6.6	5.3	3.5	14.7

Table 4. Per node RSSI, CCA and PDR (physical layer) values separated by modulation type (i.e., SUN-FSK, SUN-OQPSK and SUN-OFDM).

Table 5 shows the per-node reception probability for each independent transmission attempt (i.e., P_1, P_2, P_3) using each modulation (i.e., SUN-FSK, SUN-OQPSK and SUN-OFDM). From the data it is clear that there is no strong relationship between the modulation, the distance and the transmission attempt, except for the fact that SUN-OFDM presents the lowest mean and the highest standard deviation of all modulations. As earlier detailed, this can be explained by the fact that the SUN-OFDM transmit power is 6 dBm lower than SUN-FSK and SUN-OQPSK.

As an example, we pick nodes of the *medium* group (i.e., distance from the gateway equal to 115 m). Within that group we observe that node `56-0B` presents a high variability for SUN-OFDM transmissions, where the PDR ranges from 64.5% in the first transmission attempt to 35.9% in the third transmission attempt. Contrarily, the PDR for node `55-65` ranges from 63.1% in the first transmission attempt to 85.7% in the third transmission attempt. Hence, despite transmission attempts have a large degree of correlation for a given node and modulation given the short time interval between them, variations over 30 percent points on average can still occur.

Figure 8 shows the daily average RSSI values for each modulation and node. The shadowed region for each modulation represents the maximum and minimum values observed for each given day, and the grey shadowed area represents the days for which we do not have data. In general, the daily averages are within 10 dB, but the minimum values have drops that are over 30 dB. Since the gateway and the nodes are both fixed, such large drops in the minimal RSSI values can only be explained by the effect of moving objects within the factory.

Figure 9 shows the RSSI histogram grouped by clusters (i.e, *close*, *medium* and *far* on each row). In general, the RSSI follows a normal distribution with per-node and per-modulation mean and standard deviation values depicted in Table 5.

Figure 10 shows the per-day hourly average PDR values for each modulation and node. The shadowed region for each modulation represents the maximum and minimum values observed for each given day, and the grey shadowed area represents the days for which we do not have data. In general,

Preprints (www.preprints.org) | NOT PEER-REVIEWED | Posted: 13 February 2020 doi:10.20944/preprints202002.0174.v1

EUI-64 (2-bytes)	SUN-FSK			SUN-OQPSK			SUN-OFDM		
	P_1	P_2	P_3	P_1	P_2	P_3	P_1	P_2	P_3
56-53	68.2	77.1	69.8	70.6	79.8	76.6	70.0	71.9	64.7
55-AD	83.4	81.2	74.9	81.6	80.2	73.8	87.9	83.5	72.2
55-E4	75.4	70.9	54.2	78.0	75.2	57.7	69.7	66.4	64.4
55-99	80.4	71.8	80.6	79.7	71.1	80.2	68.3	59.2	38.2
55-DD	89.3	88.5	88.8	87.4	88.0	88.9	78.5	77.8	78.8
55-65	68.3	88.3	87.9	80.0	92.4	91.8	63.1	85.1	85.7
56-0B	68.4	80.1	74.7	69.6	79.6	75.1	64.5	63.4	35.9
56-32	94.7	92.0	95.0	90.3	87.4	90.4	80.3	77.3	79.5
55-B3	94.4	94.0	76.7	94.8	94.2	77.9	78.0	84.7	60.6
55-63	82.4	88.7	89.1	71.7	75.5	77.1	55.8	55.9	53.7
63-0A	86.6	83.5	84.3	84.2	80.5	81.9	31.7	28.1	31.9
Mean	81.0	83.3	79.6	80.7	82.2	79.2	68.0	68.5	60.5
Std. Dev.	9.5	7.5	10.9	7.8	7.0	9.1	14.3	16.1	17.7

Table 5. Per node PDR (physical layer) values separated by modulation type and packet repetition.

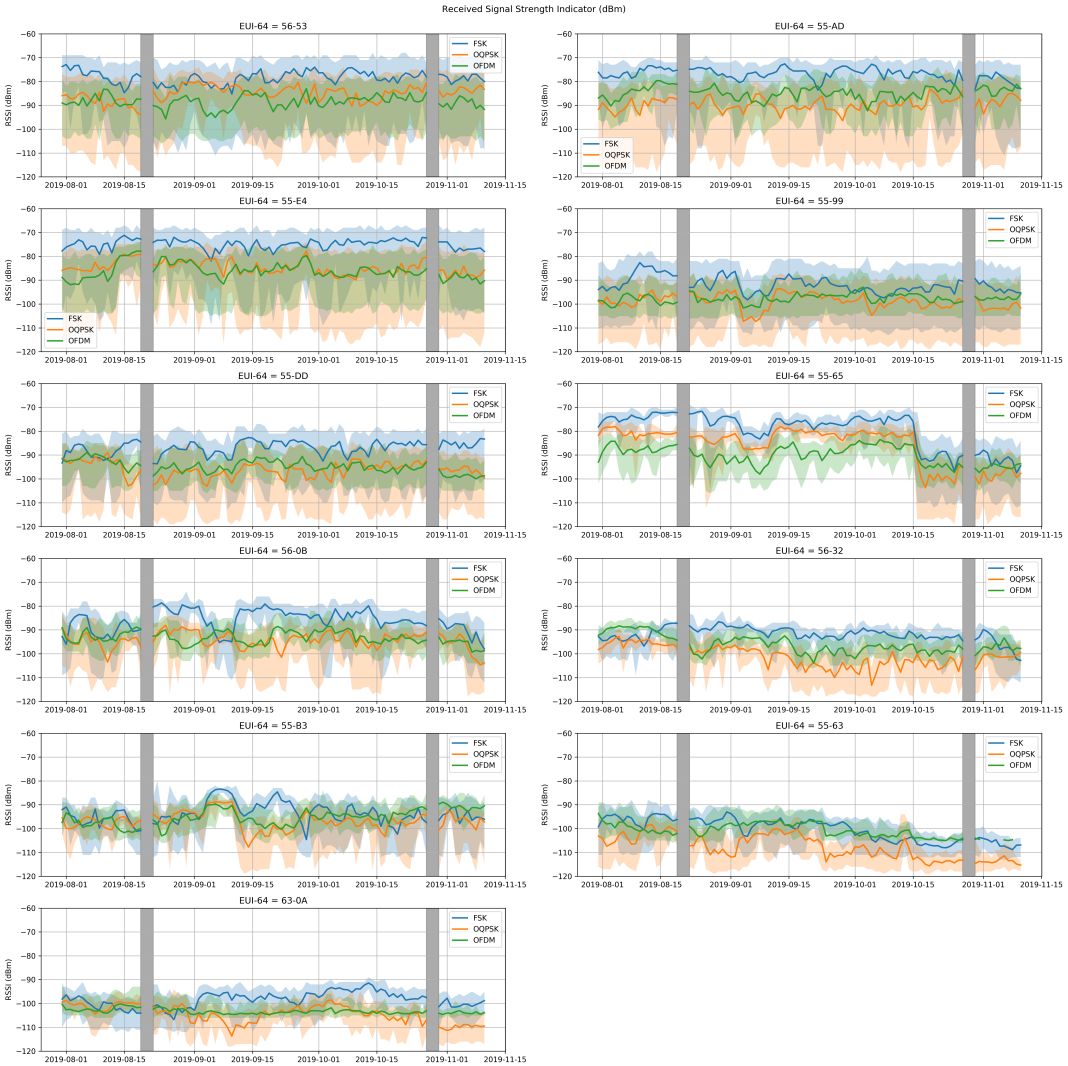

Figure 8. Per-modulation RSSI value for each node.

we observe that SUN-FSK and SUN-OQPSK modulations provide better PDR than SUN-OFDM. As mentioned above, this is owing to the fact that the link budget is better for these modulations (i.e., both higher transmit power and lower sensitivity). However, we also observe that for all modulations

Preprints (www.preprints.org) | NOT PEER-REVIEWED | Posted: 13 February 2020 doi:10.20944/preprints202002.0174.v1

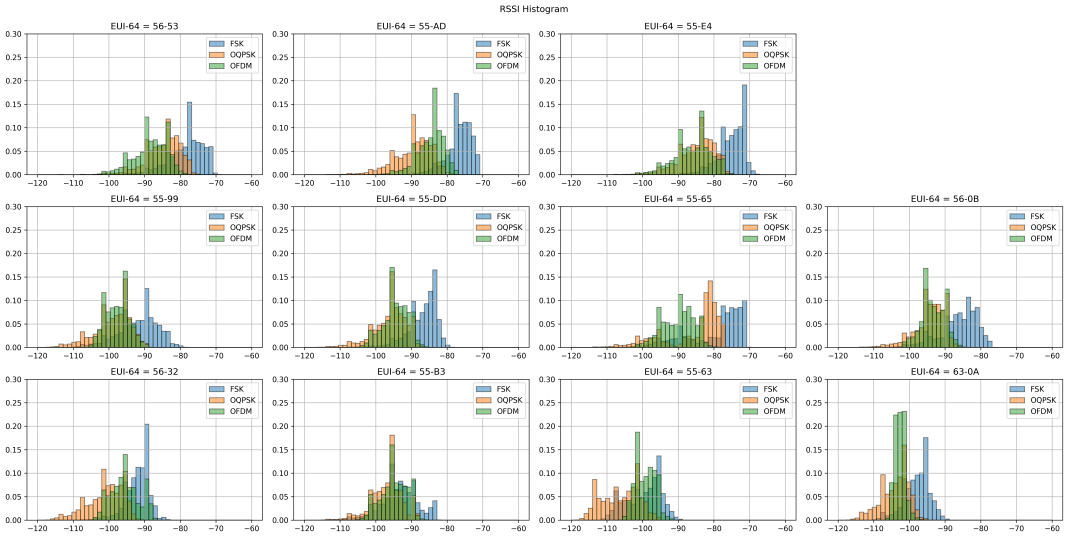

Figure 9. RSSI histogram for each node (grouped by cluster).

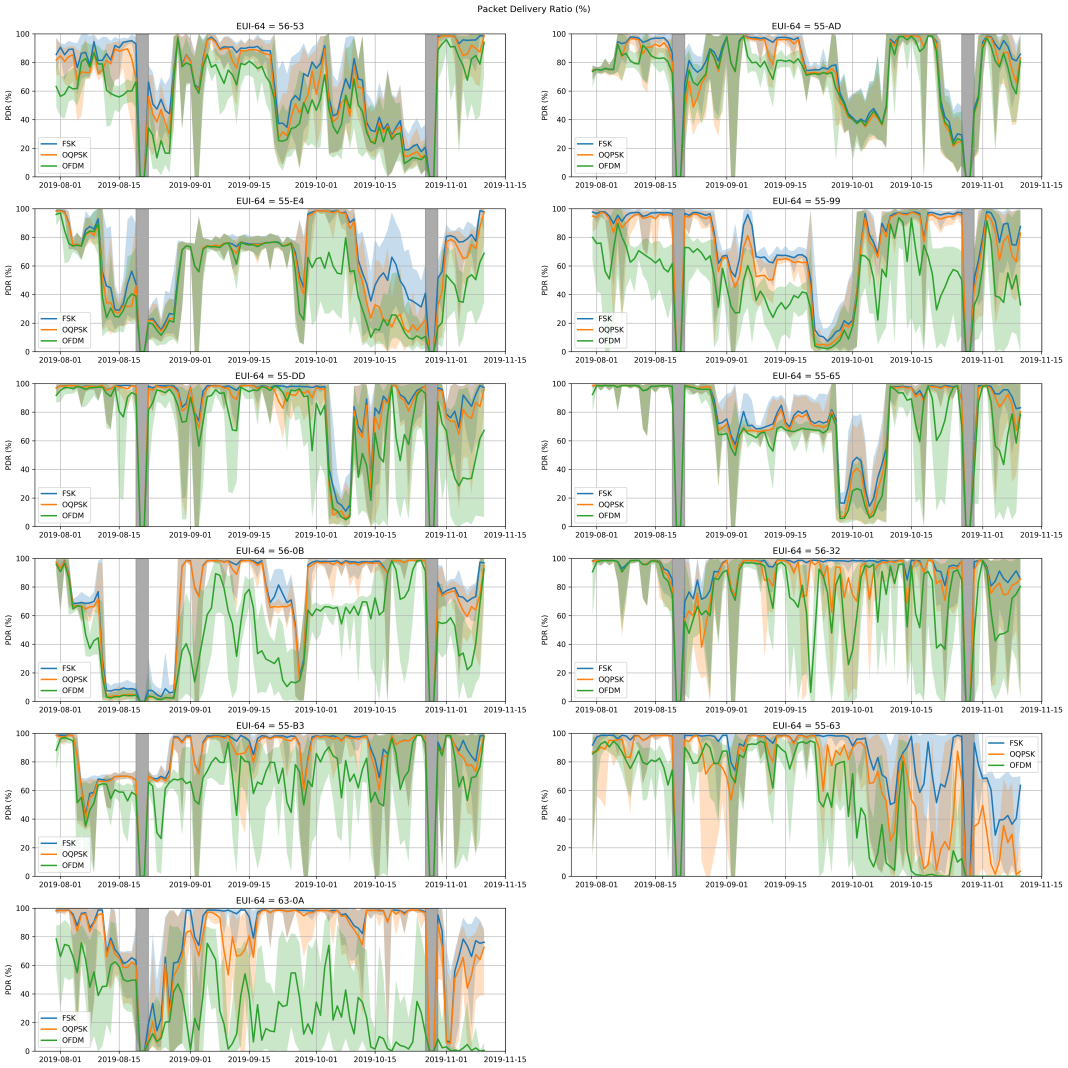

Figure 10. Per-modulation PDR value for each node.

and nodes there are sporadic drops in the average, maximum and minimum PDR values, leading to moments where nodes can experience complete loss of connectivity.

Preprints (www.preprints.org) | NOT PEER-REVIEWED | Posted: 13 February 2020 doi:10.20944/preprints202002.0174.v1

Figure 11. Per-modulation CCA value for each node.

Figure 11 shows the daily average CCA values for each modulation and node. The shadowed region for each modulation represents the standard deviation, and the grey shadowed area represents the days for which we do not have data. In general, we observe that the average CCA values for nodes in the *close* group are higher than the average CCA values of the nodes in the *medium* and *far* groups. This can be explained because the nodes are closer to the building entrance, where other wireless technologies are known to operate in the same Sub-GHz band. In addition, we observe that there are certain days where nodes experiment sporadic interference peaks of up to 5-10 dB for nodes in the *medium* and *far* groups, and 20 dB for nodes in the *close* group. Interestingly enough, such peaks do not seem to be correlated among nodes and seem to affect more the SUN-FSK and SUN-OQPSK modulations, which can be attributed to concurrent transmissions from other networks operating in the same Sub-GHz band.

Figure 12 shows the CCA histogram grouped by clusters (i.e, *close*, *medium* and *far* on each row). In general, it is interesting to observe that for nodes in the *close* group the CCA values for SUN-OFDM are spread, whereas for nodes in the *medium* and *far* groups are more concentrated. As mentioned earlier, this confirms the fact that nodes in the *close* group operate nearby the warehouse office, where other wireless technologies operating in the 868 MHz band are known to be operating.

Finally, Figure 13 shows the RSSI vs. PDR scatter plot for each modulation and node, where each point is the 8-hour average of both parameters. Contrarily to common wisdom, where nodes

Preprints (www.preprints.org) | NOT PEER-REVIEWED | Posted: 13 February 2020 doi:10.20944/preprints202002.0174.v1

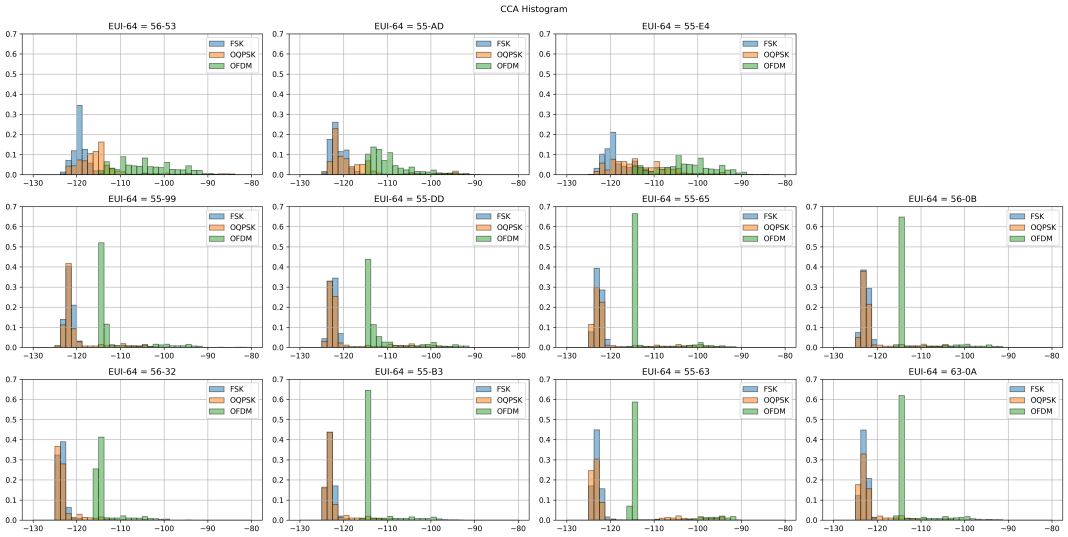

Figure 12. CCA histogram for each node (grouped by cluster).

experience *connected*, *transition* and *disconnected* zones according to their communication distance, our measurements show that PDR is not only related to distance, but largely impacted by multi-path propagation and interference. In particular, for nodes in the *close* and *medium* groups, where the average RSSI is well above the modulation sensitivity, we observe that the PDR ranges from 0% to 100% in a random pattern. In contrast, for nodes in the *far* group, we observe that the *connected*, *transition* and *disconnected* zones start to appear in the plots. This confirms the idea that nodes in the *close* and *medium* groups are limited by multi-path propagation and external interference, whereas nodes in the *far* group are limited by propagation effects.

5. Discussion

Traditional low-power wireless communications in the industrial domain have been based on the IEEE 802.15.4 standard, using the OQPSK-DSSS modulation and operating in the 2.4 GHz ISM (Industrial, Scientific and Medical) band. Given the expected communication range (i.e., typically below 50 meters) caused by propagation and interference effects, networks based on such standard have typically relied on mesh technologies, which allow to extend the range by forwarding neighbor packets towards the gateway in a multi-hop fashion. However, deploying and maintaining mesh networks has proven to be challenging due to the changing nature of the environment.

Thanks to the deployment in a real-world industrial setting, in this paper we have shown that the use of the Sub-GHz band combined with the robust IEEE 802.15.4-2015 SUN modulations provides good communication characteristics in an industrial setting, with links up to 273.5 meters, using a transmission power between 9 dBm and 15 dBm, and providing effective data rates of 50 kbps. This allows to simplify network deployment and operation compared to mesh networks based on the traditional IEEE 802.15.4 standard. However, despite the propagation and robustness advantage compared to traditional IEEE 802.15.4 communications, we have observed that communications between the nodes and the gateway are still severely impacted by both propagation and interference effects, limiting network performance in terms of predictability and availability. In fact, the average PDR is only 75.9%, which is well below the typical 99.9% requirement for industrial settings.

To cope with packet losses caused by such propagation and interference effects, we have used blind packet repetitions, a common technique used to increase reliability of LR-WPAN (e.g., WirelessHART, ISA 100.11a, 6TiSCH) [19] and LPWAN (e.g., LoRaWAN, Sigfox, NB-IoT, etc.) [20] networks. However, the results from our deployment show that even 3 transmissions cannot guarantee 99.9% delivery. In fact, with 3 transmissions it is only possible to reach an average of 94.2% with SUN-FSK, 94.1% with SUN-OQPSK, and 86.0% with SUN-OFDM, which is still far from the target requirement. Further

Preprints (www.preprints.org) | NOT PEER-REVIEWED | Posted: 13 February 2020 doi:10.20944/preprints202002.0174.v1

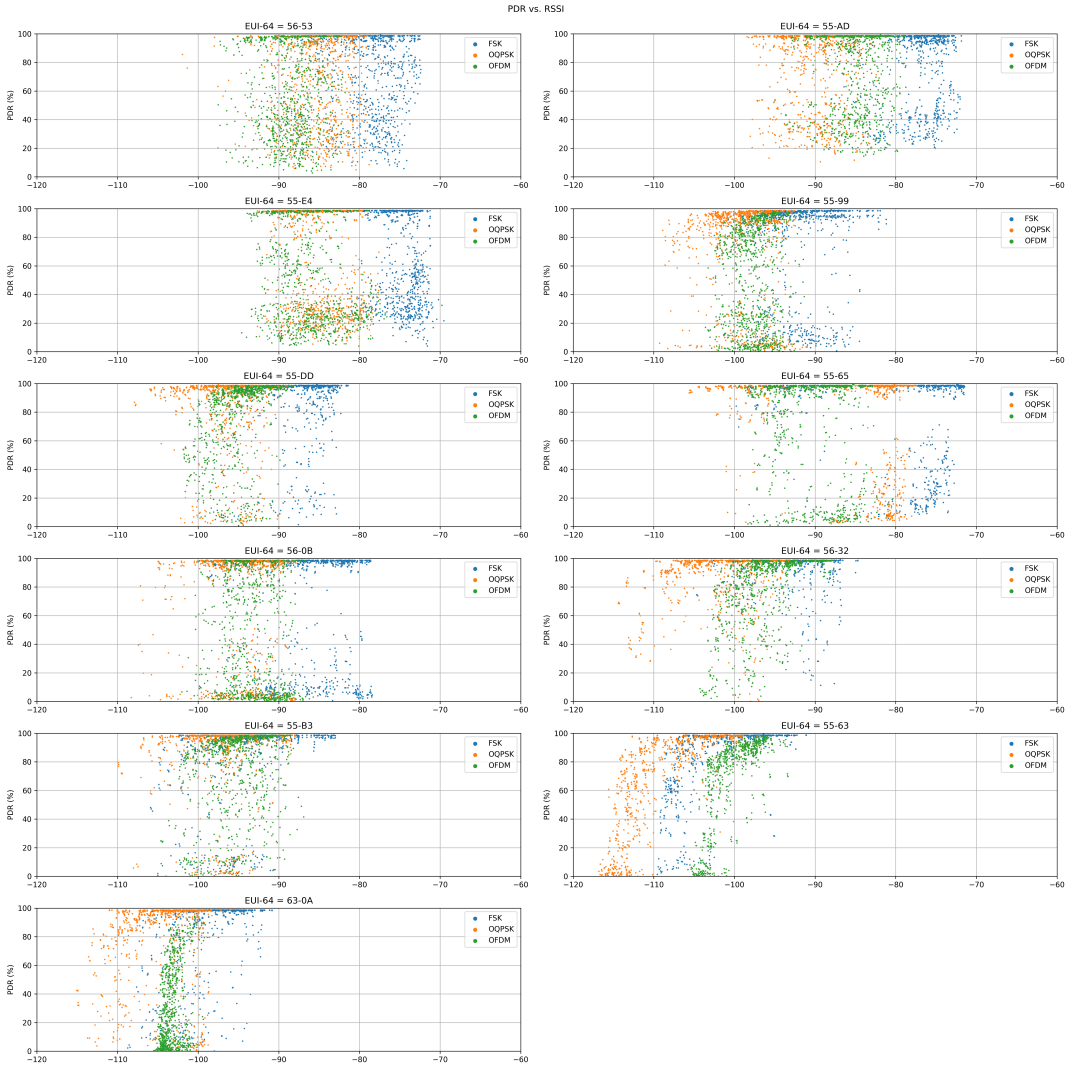

Figure 13. Per-modulation RSSI vs. PDR values for each node.

increasing delivery success adding more transmissions is possible, but it has a high impact to the battery life and is limited by duty-cycle regulations, as it causes interference to the remaining nodes, as well as to other networks operating in the same area.

A widely used technique to further mitigate the propagation and interference effects is frequency diversity (i.e., channel hopping). But, while frequency diversity is suitable in the 2.4 GHz band given that the available bandwidth is large and channels are uncorrelated, the benefits in the Sub-GHz band (i.e., 868 MHz in Europe and 915 MHz in United States) are mostly limited to mitigating interference effects. In addition, adding frequency diversity requires synchronization between the nodes and the gateway, which adds complexity to the solution and limits certain use cases where there are multiple gateways and/or nodes are mobile.

Interestingly, modulation diversity (i.e., changing modulations for every transmitted packet) has the potential of providing similar effects as frequency diversity, since each modulation has its own properties with regard to robustness against both propagation and interference effects. For example, narrow-band modulations (i.e., SUN-FSK) are robust and provide a large number of channels, but are prone to frequency drifts caused by temperature changes and component ageing. In contrast, wide-band modulations (i.e., SUN-OQPSK) are inherently robust to narrow-band interference and can cope better with frequency drift, but have a limited number of channels available. Finally, multi-carrier modulations (i.e., SUN-OFDM) can use time and frequency repetition to provide robustness against

both multi-path fading and external interference effects, while providing a trade-off in terms of channels available. Hence, using different modulations for packet re-transmissions can be used as a mechanism to address scenarios where nodes are subject to multi-path propagation and where multiple wireless technologies coexist in the same band.

Until today, modulation diversity has been limited in low-power wireless communications due to the lack of standards and the availability of commercial transceivers. However, the IEEE 802.15.4-2015 standard included the definitions of the IEEE 802.15.4g amendment, which proposes a variety of physical layers, covering a wide variety of frequency bands, to meet the requirements of different types of applications. In addition, off-the-shelf transceivers that implement all the physical layer definitions of this standard are now available, which allows the nodes to use different modulation schemes using only one radio transceiver. Thus, modulation diversity may now be used to deal with the different challenges of low-power wireless communications that need to be faced in industrial environments.

6. Conclusions

In this article we have presented a long-term deployment in a real-world industrial environment using the SUN modulations, as introduced in the IEEE 802.15.4-2015 standard. The resulting dataset shows that despite the increased range (i.e., links up to 273.5 m), the use of such modulations alone cannot guarantee the dependability requirements of industrial and smart grid applications (i.e., PDR>99%) due to propagation and interference effects. Taking that into account, in the future we aim to use the dataset as a tool to explore the suitability of combining packet replication with modulation diversity to increase PDR while meeting the node and regulatory constraints, i.e., energy expenditure and duty cycling. This goal is aligned with the objectives defined by the RAW (Reliable and Available Wireless) WG (Working Group) at the IETF (Internet Engineering Task Force), in which protocols to manage diversity will be developed as a tool to ensure dependable wireless communications.

Author Contributions: Pere Tuset-Peiró has conducted the experiments, analyzed the data and contributed to writing the manuscript. Ruan D. Gomes has contributed to analyzing the data and writing the manuscript. Pascal Thubert has contributed to writing the manuscript. Xavier Vilajosana has contributed to conceptualizing the experiments, supervising the project and reviewing the manuscript.

Funding: This research is partially supported by the Generalitat de Catalunya (SGR-60-2017) and Spanish Ministry of Science, Innovation and Universities (SPOTS RTI2018-095438-A-I00) grants. This project is co-financed[2] by the European Union Regional Development Fund within the framework of the ERDF Operational Program of Catalonia 2014-2020 with a grant of 50% (€2M) of total cost eligible (€4M). The author Ruan D. Gomes also has the support of the Brazilian National Council for Scientific and Technological Development (CNPq).

Conflicts of Interest: The authors declare no conflict of interest.

References

1. Bartolomeu, P.; Alam, M.; Ferreira, J.; Fonseca, J.A. Supporting Deterministic Wireless Communications in Industrial IoT. *IEEE Transactions on Industrial Informatics* **2018**, *14*, 4045–4054. doi:10.1109/TII.2018.2825998.
2. Baccour, N.; Koubundefineda, A.; Mottola, L.; Zúñiga, M.A.; Youssef, H.; Boano, C.A.; Alves, M. Radio Link Quality Estimation in Wireless Sensor Networks: A Survey. *ACM Trans. Sen. Netw.* **2012**, *8*. doi:10.1145/2240116.2240123.
3. Thubert, P.; Cavalcanti, D.; Vilajosana, X.; Schmitt, C. Reliable and Available Wireless Technologies. Internet-Draft draft-thubert-raw-technologies-04, IETF Secretariat, 2020. http://www.ietf.org/internet-drafts/draft-thubert-raw-technologies-04.txt.
4. Koutsiamanis, R.A.; Papadopoulos, G.; Jenschke, T.L.; Thubert, P.; Montavont, N. Meet the PAREO Functions: Towards Reliable and Available Wireless Networks. 2020 IEEE International Conference on Communications (ICC), 2020.

[2] Aquest projecte està cofinançat pel Fons Europeu de Desenvolupament Regional de la Unió Europea en el marc del Programa Operatiu FEDER de Catalunya 2014-2020 amb un ajut del 50% (2M€) del cost total elegible (4M€).

5. IEEE Standard for Low-Rate Wireless Networks. *IEEE Std 802.15.4-2015 (Revision of IEEE Std 802.15.4-2011)* **2016**, pp. 1–709. doi:10.1109/IEEESTD.2016.7460875.
6. Kuor-Hsin Chang.; Mason, B. The IEEE 802.15.4g standard for smart metering utility networks. 2012 IEEE Third International Conference on Smart Grid Communications (SmartGridComm), 2012, pp. 476–480. doi:10.1109/SmartGridComm.2012.6486030.
7. Mochizuki, K.; Obata, K.; Mizutani, K.; Harada, H. Development and field experiment of wide area Wi-SUN system based on IEEE 802.15.4g. 2016 IEEE 3rd World Forum on Internet of Things (WF-IoT), 2016, pp. 76–81. doi:10.1109/WF-IoT.2016.7845425.
8. Sum, C.S.; Zhou, M.T.; Kojima, F.; Harada, H. Experimental Performance Evaluation of Multihop IEEE 802.15.4/4g/4e Smart Utility Networks in Outdoor Environment. *Wireless Communications and Mobile Computing* **2017**, *2017*, 1–13. doi:10.1155/2017/7137406.
9. Muñoz, J.; Chang, T.; Vilajosana, X.; Watteyne, T. Evaluation of IEEE802.15.4g for Environmental Observations. *Sensors* **2018**, *18*. doi:10.3390/s18103468.
10. Muñoz, J.; Riou, E.; Vilajosana, X.; Muhlethaler, P.; Watteyne, T. Overview of IEEE802.15.4g OFDM and its applicability to smart building applications. 2018 Wireless Days (WD), 2018, pp. 123–130. doi:10.1109/WD.2018.8361707.
11. IEEE Standard for Local and metropolitan area networks–Part 15.4: Low-Rate Wireless Personal Area Networks (LR-WPANs) Amendment 1: MAC sublayer. *IEEE Std 802.15.4e-2012 (Amendment to IEEE Std 802.15.4-2011)* **2012**, pp. 1–225. doi:10.1109/IEEESTD.2012.6185525.
12. IEEE Standard for Local and metropolitan area networks–Part 15.4: Low-Rate Wireless Personal Area Networks (LR-WPANs) Amendment 3: Physical Layer (PHY) Specifications for Low-Data-Rate, Wireless, Smart Metering Utility Networks. *IEEE Std 802.15.4g-2012 (Amendment to IEEE Std 802.15.4-2011)* **2012**, pp. 1–252.
13. Vilajosana, X.; Tuset, P.; Watteyne, T.; Pister, K. OpenMote: Open-Source Prototyping Platform for the Industrial IoT. Ad Hoc Networks; Mitton, N.; Kantarci, M.E.; Gallais, A.; Papavassiliou, S., Eds.; Springer International Publishing: Cham, 2015; pp. 211–222.
14. Tuset-Peiró, P.; Vilajosana, X.; Watteyne, T. OpenMote+: A Range-Agile Multi-Radio Mote. Proceedings of the 2016 International Conference on Embedded Wireless Systems and Networks; Junction Publishing: USA, 2016; EWSN '16, pp. 333–334.
15. Texas Instruments. *CC2538 Powerful Wireless Microcontroller System-On-Chip for 2.4-GHz IEEE 802.15.4, 6LoWPAN, and ZigBee® Applications (Rev. SWRS096D)*, 2015.
16. Atmel. *AT86RF215 Device Family: Sub-1GHz/2.4GHz Transceiver and I/Q Radio for IEEE Std 802.15.4-2015 (Rev. 42415E)*, 2016.
17. Bosch. *BME280: Combined humidity and pressure sensor (BST-BME280-DS002-15)*, 2018.
18. Texas Instruments. *OPT3001: Ambient Light Sensor (SBOS681C)*, 2017.
19. d. Armas, J.; Tuset, P.; Chang, T.; Adelantado, F.; Watteyne, T.; Vilajosana, X. Determinism through Path Diversity: Why Packet Replication Makes Sense. 2016 International Conference on Intelligent Networking and Collaborative Systems (INCoS), 2016, pp. 150–154. doi:10.1109/INCoS.2016.105.
20. Haxhibeqiri, J.; De Poorter, E.; Moerman, I.; Hoebeke, J. A Survey of LoRaWAN for IoT: From Technology to Application. *Sensors* **2018**, *18*. doi:10.3390/s18113995.